Contrat CNES Année 2020
Développement de la Mars Climate Database et soutien du programme EXOMARS
BC : 4500067205 / DSO091

Note technique sur l'amélioration du cycle des poussières dans le GCM

Ref : LMD_CNES_EXM_2020_gcm_dust

Préparé par : Antoine Bierjon, Ehouarn Millour, Francois Forget, Margaux Vals

Laboratoire de Météorologie Dynamique, CNRS, IPSL, Paris, France.

15 décembre 2020

Contents

1 Introduction **3**

2 The 3 parametrizations ruling the GCM dust cycle **4**

3 Observations and GCM validation method **8**

4 Parametrizations tuning campaign **16**

5 An unresolved mystery : the high-altitude storm dust **24**

6 Dust scaling mode **25**

7 Conclusion **28**

1 Introduction

This document reviews the updates concerning the dust cycle in the Martian Global Climate Model version 6 and the related work that has been carried throughout the year 2020.

The previous report LMD_CNES_EXM_gcm6.0 from 2019 had emphasized and detailed three parametrizations that govern the new GCM dust cycle. The first one is the revisited dust injection scheme, meticulously driven by observational scenarios, which replaces the former two-step approach consisting of a huge constant injection, followed by a strong renormalization to the observations. As the second keystone of this new dust cycle, the mesoscale phenomenon of the *rocket dust storms*, revealed by Spiga et al. [2013] and very active in the dusty season, had been implemented by Chao Wang (Wang et al. [2018]) and Margaux Vals, and profoundly redesigns the dust vertical distribution. The last part of this triptych was another mesoscale process, induced by the subgrid-scale topography's updraft slope winds that concentrate aerosols on top of the mountains, and enable dust to follow a *rocket dust storm*-like local ascension. This process, designated more simply as *slope winds*, had been parametrized by Margaux Vals during her PhD thesis. **Section 2** underlines some aspects of these parametrizations which our 2020 work is based on. We also make a little update on the aerosols scavenging process by the CO_2 condensation in the polar night, introduced in the previous report.

Compared to last year, improvements have been made on the use of observation datasets, as well as the diagnostics and validation of the GCM. This was made possible via the development of an observer simulator adapted to the Mars Climate Sounder observations from the Mars Reconnaissance Orbiter, whose data constitute the main element of comparison and validation for the GCM dust cycle. This MCS simulator, associated with relevant diagnostic output variables from the GCM, enables us to see the GCM atmosphere like the instrument and thus to better constraint the model through the comparison with the real observations. In order to complete and ascertain MCS observations, especially concerning the *dust detached layers* hardly reproduced by GCMs, we also began to work on solar occultation data from the NOMAD instrument onboard ExoMars Trace Gas Orbiter. Our work on observations and GCM diagnostics is detailed in **Section 3**.

With these enhanced validation tools, we performed a tuning campaign on the parametrizations from Section 2, partially based on what we had learnt from previous tuning campaigns (see report LMD_CNES_EXM_gcm6.0). Our studies, explained in **Section 4**, focused on four parameters that play a major role on the GCM dust cycle, and tested a variety of their combinations. This study brought good constraints on each parameter, however it also exposed some behaviours, common to every GCM simulations, that are intriguing in regard to the observations and the current knowledge on Mars climate. One of these behaviours is the presence of dust particles at high altitudes of 60-80km, entirely sustained by the rocketdust-storm scheme. This particular subject is developped in its own **Section 5**.

These persisting discrepancies with observations led us to establish a new strategy in order to temper the influence of the dust cycle on the other components of the GCM climate system. When computing the radiative impact of the dust particles, we rescale it towards more realistic values using the ratio of the column-integrated optical depths of the GCM and the observation scenario. This approach shares similarities with the former GCM5.3-like semi-interactive or "*tauscaling*" method. Nonetheless, as described in **Section 6**, the way we implement this method has the

advantage of letting the daily dust cycle freely evolve around the constrained local time of 14h. The ratio used here may also serve as a figure of merit to evaluate the good tuning of the GCM dust processes against the observations, with a possibility to make it tend towards unity.

2 The 3 parametrizations ruling the GCM dust cycle

In this section, we remind some relevant points about parametrizations that were already detailed in previous reports (notably LMD_CNES_EXM_gcm6.0). The double goal of this new dust cycle with regard to the former version is to get a more realistic simulated dust vertical distribution, especially with the representation of the "*dust detached layers*" observed at every season by MCS, while letting the dust be more "freely" driven by the physical processes.

Dust injection scheme. The new dust injection scheme, developped in 2017 by Deborah Bardet, takes in input a prescribed column dust optical depth (CDOD), which is compared to the optical depth computed by the GCM. Usually, the prescribed CDOD is taken from mapped scenarios made by Luca Montabone (see Montabone et al. [2015], Montabone [2020] and Figure 1). These scenarios cover Martian Years from MY24 to MY35, and gather on a regular horizontal grid the observations from different instruments (TES[1], THEMIS[2], MCS[3]) which are then extrapolated to cover the whole planet via a kriging procedure, and are normalized to a reference surface pressure of 610Pa.

When read by the GCM, the prescribed normalized column dust opacity *tau_pref_scenario* is recalibrated from infrared absorption to visible extinction via a multiplicative factor of 2.6 to be comparable with the model's own visible CDOD, *tau_pref_gcm*[4].

For the implementation concerns, we consider the scenarios to be representative of the certain local time of 14h, which is close from the daytime Mean Solar Local Time of the heliosynchronous orbits of the instruments. When a local grid point of the model reaches this local time, we compute the difference between the current *tau_pref_gcm* and the *tau_pref_scenario* from the next day at 14h. The difference, if positive (more dust in the observations than in the model), gives us the amount of dust that has to be injected in the model to reach the prescribed column one day later. The conversion from the tau difference into the dust flux injected from the surface in the first atmospheric layer (in $\mathrm{kg}_{dust}.\mathrm{m}^{-2}.\mathrm{s}^{-1}$) is made via the following relationship :

$$\Delta q = \frac{4}{3}\frac{p_{surf}}{p_{ref}}\frac{\rho_{dust}\ r_{\mathrm{eff}}}{Q_{\mathrm{ext}}\ \Delta t}\ \Delta\tau \tag{1}$$

with p_{surf} the local surface pressure (in Pa) and p_{ref} the reference pressure (610 Pa) ; ρ_{dust} the dust density, r_{eff} the effective radius (meters) and Q_{ext} the visible extinction coefficient of the injected dust distribution (resp. fixed at $2500\mathrm{kg}_{dust}.\mathrm{m}^{-3}$, 3µm and 2.4) ; and $\Delta t = t_{end\ of\ inj.} - t_{start\ of\ inj.}$ (in s) the local time interval during which the injection is performed at a constant rate. A tunable proportionality coefficient is also added (the reasons behind this coefficient are explained in Section 4).

[1] *Thermal Emission Spectrometer*, onboard Mars Global Surveyor
[2] *Thermal Emission Imaging System*, onboard Mars Odyssey
[3] *Mars Climate Sounder*, onboard Mars Reconnaissance Orbiter
[4] This value of 2.6 and the associated hypotheses and uncertainties are detailed in Montabone et al. [2015]

If the tau difference is negative (more dust in the model than in the observations), nothing is done, and the dust freely evolves with the dynamics, the sedimentation, or as part of the condensable species' cycles (water and CO_2).

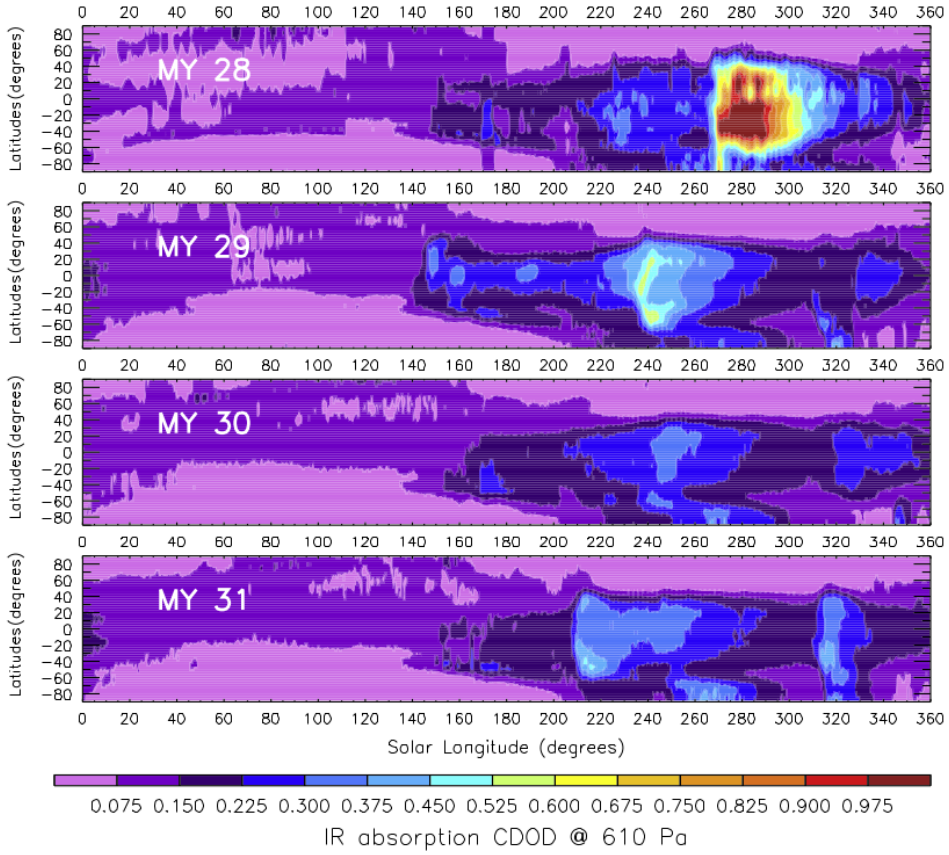

Figure 1: Zonal means of 9.3µm absorption column dust optical depth scenarios (normalized to 610 Pa) as a function of solar longitude and latitude for Martian Years MY28 to MY31, calculated using the regularly gridded maps after the application of the kriging procedure. *Credits : Montabone et al. [2015]*

Rocket dust storm. Spiga et al. [2013] had revealed that locally concentrated dust can create on a subgrid scale some powerful radiatively-driven convective cells that lift the particles very high in the atmosphere : the *rocket dust storm* phenomenon.

In the GCM, we implement this process via a new tracer, the *stormdust*, that is distinct from the usual background dust tracer. The quantity of stormdust present in each atmospheric column enables us to define, thanks to the reference mixing ratio of an observed local dust storm, a mesh fraction in which we consider that all the stormdust is concentrated. When any layer of the subgrid fraction contains a sufficient ratio of stormdust mass over background dust, we trigger the rocket dust storm scheme.

Indeed, in this mesh fraction, the additional opacity induced by the presence of stormdust, compared to the rest of the mesh, generates a stronger radiative heating on the surrounding air. This air parcel locally rises under the influence

of flottability, taking along the dust particles. A conservative Van Leer scheme (Van Leer [1977], Hourdin and Armengaud [1999]) is used for the transport of the advected dust. During its ascension, some of the stormdust is detrained horizontally, and is transformed into background dust. The Figure 2, taken from Wang et al. [2018], shows the quadratic relationship that links the vertical radiatively-induced speed of the parcel and the horizontal detrainment coefficient. When the vertical velocity becomes too low in a layer, or when there is not enough stormdust to trigger a storm, all the stormdust of the layer is detrained into background dust. A tunable multiplicative factor is also put before the detrainment coefficient.

In practice, the GCM uses two ways to create stormdust tracer. The main one is by coupling the rocket dust storm and the injection schemes : the type of dust that is injected in the first layer is stormdust. This choice is relevant since the need of injection in the model generally corresponds to the apparition of a local dust storm in the scenarios. The stormdust type of the injected tracer enables the vertical advection of the dust particles, like during a dust storm. Furthermore, since Margaux Vals's work, the amount of background dust that is present in the storm fraction of the mesh and also entrained by the updraft, is converted into stormdust, and contributes to sustain the storm at higher layers.

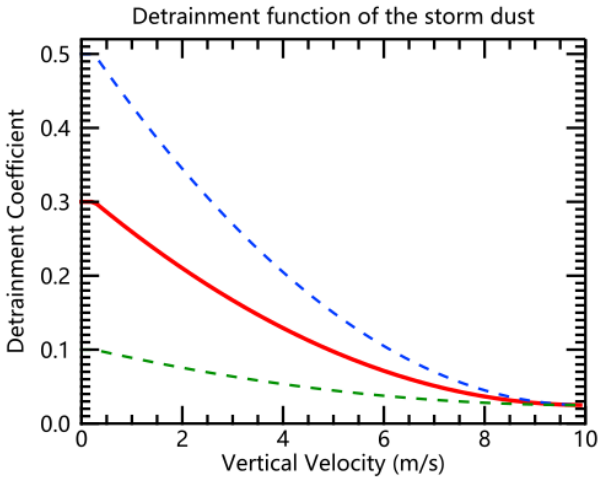

Figure 2: Detrainment coefficient of stormdust in function of the vertical velocity, with different multiplicative factors. The stronger the wind, the weaker the detrainment. *Credits : Wang et al. [2018]*

Slope winds. The "*slope winds*" parametrization encompasses multi-step mesoscale physical processes that occur in proximity of a local orographic summit. The influence zone of this summit is defined by the convergence of the anabatic winds that build up during the day and entrain the aerosols from the boundary layer up above the moutain's top. The background dust that gets concentrated high up is converted into a new tracer, called *topdust*, and radiatively heats up the air locally. As a result, a *rocketduststorm*-like scheme takes place : the heated air induces a new ascending motion by flottability, which transports the dust particles even higher before it detrains back into the environment, out of the ascending column.

In practice, the upslope winds this process originates from depend on the slope and the height of the mountain, so we assign to each grid mesh their greatest local

height (from base to top) h_{mons}, and the mesh fraction in which the ascending column takes place is arbitrarily set to :

$$x_{mons} = C_{mons} \frac{h_{mons} - h_{min}}{h_{max} - h_{min}} \tag{2}$$

with h_{min} and h_{max} respectively the lowest and highest value of h_{mons} all around the globe, and C_{mons} a tunable coefficient put at 0.5 by default since the last tests from Margaux Vals (see report LMD_CNES_EXM_gcm6.0).

Unlike the rocket dust storms that almost exclusively happen in the dusty season, when Mars is closer to the Sun, the slope winds entrainment of dust takes place all year long and maintains a *dust detached layers*, even if it lies a bit lower in altitude than those observed by MCS.

Scavenging aerosols with the CO2 ice. The previous report had also introduced the new representation of the scavenging of aerosols (dust, water ice) when the atmospheric CO_2 uses them as condensation nucleii. When falling down, the CO_2 snowflakes can also encounter a warm enough layer to sublimate and release their core aerosol particle in the air. This whole process, particularly important in the polar nights where the temperature reaches the CO_2 freeze point, is controlled in the model by only one parameter called the "*scavenging ratio*" R. This ratio can be specific to each aerosol type, and accounts for the aerosol's concentration within the CO_2 ice particles over its atmospheric concentration. Observations on Earth give a broad range of values for this ratio in water clouds, from 10 to 1000, and it is fixed in the Mars GCM at a constant value of 100 for now.

The implementation of the scavenging by the CO_2 ice has shown promising behaviours in dampening the accumulation of dust in the polar regions, especially above the Northern polar cap (see Figure 3). A finer evaluation of the scavenging ratios could be performed, firstly by using observations of aerosols in the polar night from the instrument PFS[5], whose climatology has recently been made available by Giuranna et al. [2019] ; furthermore, with the help of the CO_2 microphysics model being developped at LATMOS[6] by Christophe Mathé and Anni Määttänen.

However, the three parametrizations summarized above had a first order effect on the global dust horizontal transport, which can generate a huge variability between simulations on the dust polar concentration. It has thus been decided to put on standby the tuning of the scavenging by CO_2, and to focus on the global dust cycle improvement before dealing specifically with the polar latitudes.

[5] *Planetary Fourier Spectrometer*, onboard Mars Express
[6] Laboratoire Atmosphères, Milieux, Observations Spatiales

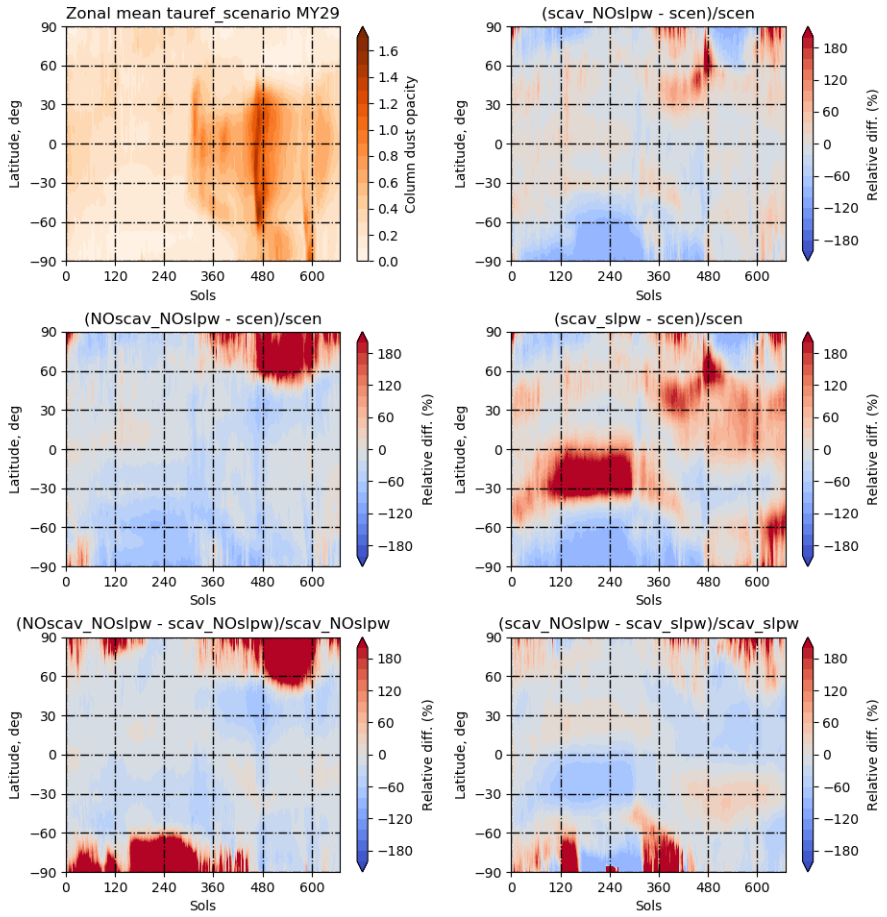

Figure 3: L_S-latitude maps of zonal mean visible column-integrated dust optical depth from scenario and simulations of MY29. **Top, left:** Absolute value of the scenario. **Top, right:** Relative difference of a simulation with scavenging by CO_2 (R=100) and no slope winds, to the scenario. **Middle, left:** Relative difference of a simulation with neither scavenging by CO_2 nor slope winds, to the scenario. **Middle, right:** Relative difference of a simulation with both scavenging by CO_2 (R=100) and slope winds, to the scenario. **Bottom, left:** Relative difference of the simulation with neither scavenging by CO_2 nor slope winds, to the simulation with scavenging by CO_2 (R=100) and no slope winds. **Bottom, right:** Relative difference of the simulation with scavenging by CO_2 (R100) and no slope winds, to the simulation with both scavenging by CO_2 (R=100) and slope winds.

3 Observations and GCM validation method

As mentionned in Section 2, we use the observations of the Martian atmosphere to drive the GCM online, i.e. as inputs for parametrizations. On the other hand, they constitute the main source of the *a posteriori* validation of the model. As far as the dust cycle is concerned, and especially the dust vertical distribution, the Mars Climate Sounder data has been our principal reference for many years now. During this year, we worked on improving our use of this abundant data and to reduce the uncertainties coming from our comparison method. This implies : a

better matching of the spatial and temporal distribution of the GCM outputs to the MCS observations, which can be done thanks to the developpement of an observer simulator ; besides, a good choice of the diagnostic variables used to compare the GCM simulated dust with MCS dust retrievals. Knowing the strong radiative effect of the dust aerosol on the Mars atmosphere, not only did we consider variables quantifying the presence of dust, but also the temperature, retrieved by MCS as well.

Moreover, in order to diversify our observational references for the validation of the dust cycle, we have also looked at the new aerosol retrievals from NOMAD[7], a spectrometer suite onboard ExoMars Trace Gas Orbiter, and especially searched for colocalized observations between NOMAD and MCS.

Last but not least, since the GCM column dust opacity is not renormalized to the scenario anymore, the comparison of *tau_pref_gcm* and *tau_pref_scenario* also has become an element of validation.

MCS observation files. The instrument Mars Climate Sounder is a mid- and far-infrared thermal emission radiometer performing nadir and limb soundings of the atmosphere (Kleinböhl et al. [2009]). Its carrier, the Mars Reconnaissance Orbiter, is in heliosynchronous orbit around the planet, with 2 overflights of the equator per day, at the Mean Solar Local Times of 3h and 15h, and offers a multi-annual coverage of Mars atmosphere. The main level 2 retrievals, inverted from the measured radiances, are the pressure P, temperature T, and extinction opacities of dust (at 21.6µm) and water ice (at 11.9µm) $d_z\tau$ (in km^{-1}).

From this retrieved variables, one can build the density-scaled opacity (DSO) of the aerosols, expressed in m^2.kg^{-1}, more easy than opacity to manipulate vertical profiles :

$$DSO = \frac{d_z\tau}{\rho} = \frac{d_z\tau \; r \; T}{P} \tag{3}$$

with $r = \frac{R}{M_{atm}} = 191$ J.kg^{-1}.K^{-1} and $d_z\tau$ converted in m^{-1}. It is then possible to draw a climatology of the *dust detached layers*, as depicted on Figure 4.

To be easier to handle, the soundings have been recasted by the MCS team on a unique vertical axis of 105 pressure levels, ranging from 1878.9 to 0.004247Pa. Then, all the profiles have been gathered by Luca Montabone (Montabone [2020]) in bins of 5° of L_S, on a 64x48 horizontal grid. At every point on the horizontal grid, one L_S bin thus contains profiles from several days, measured at different local times that can greatly vary from the Mean Solar Time of 3h and 15h (especially at high latitudes). The binning is also specific to each variable[8], and the daytime and nighttime[9] measurements are stored separately. Because of the instrument calibration, daytime dust retrievals are less reliable than nighttime ones, according to Heavens et al. [2011a].

MCS observer simulator. Previously, the comparisons of the GCM simulations with these MCS binned files were done as follows, with the use of offline utility programs we developped beside the GCM : after one program recasting the GCM outputs on the MCS pressure vertical axis, another program would reinterpolate the GCM files at the local times of 3h and 15h all around the globe, and a third one would smooth the values by averaging them in L_S bins similar to the MCS bins of 5°L_S. This post-processing enabled the GCM simulations to get quite comparable to the MCS files.

[7] *Nadir and Occultation for MArs Discovery*

[8] for example, there are more retrievals of the temperature than the dust or water ice opacities

[9] average local time of measure comprised between [6h;18h] for daytime, and between [18h;6h] for nighttime

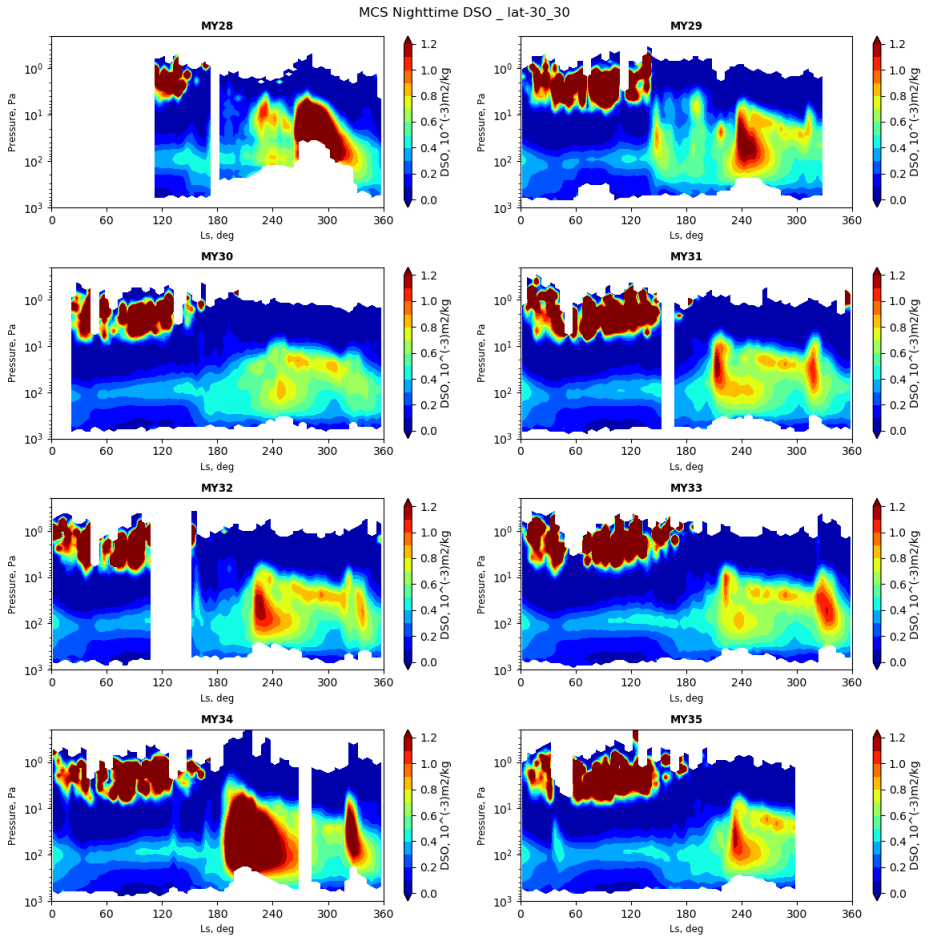

Figure 4: Nighttime Dust Density-Scaled Opacity at 21.6µm, retrieved by MCS during every Mars Year - Zonal & meridional average in latitudinal band of [-30°N;30°N]. *NB : the very high DSO in the first half of the years are not to be attributed to dust but to CO_2 according to Heavens et al. [2011b]*

However, this method implied three temporal deviations (see also Figure 5) :

- as already said, the average local time of the observations bin strongly diverges from 3h/15h the more we go towards high latitudes ;
- the variability of the local times within one bin also strongly increases at high latitudes, hence making the interpolation at only one local time may not be representative enough ;
- the prescribed local times of 3h/15h are Mean Solar Time, while the Local True Solar Time (equal to 12h when the Sun is at its zenith, and used in the GCM) at which MRO passes the equator varies during the year accordingly to the *equation of time*. The Local True Solar Time of the daytime observations at the equator can thus lie between 14.3h and 15.88h for instance.

and wasn't representative of the 3 binnings available for each retrieved variable : temperature, dust and water ice.

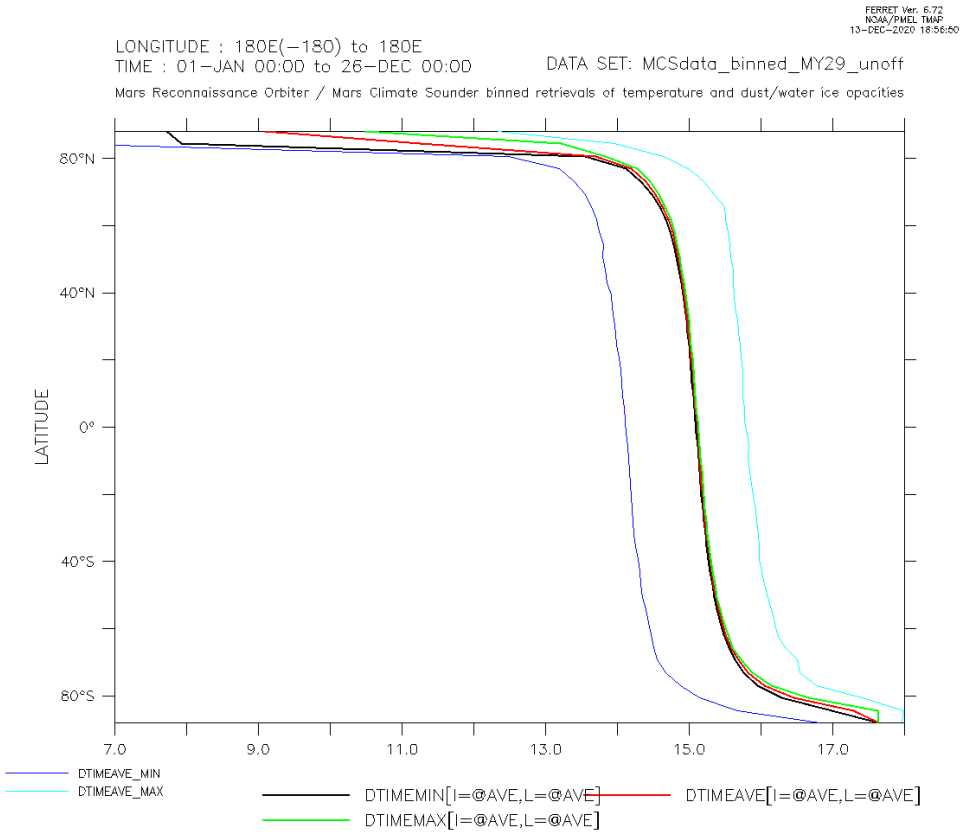

Figure 5: MCS zonal and temporal MY29 average of : **Black** : minimum local time in daytime bin *dtimemin* ; Red : average local time in daytime bin *dtimeave* ; Green : maximum local time in daytime bin *dtimemax*. Also, in blue and cyan, zonal and temporal MY29 minimum and maximum of *dtimeave*

Therefore, we decided to develop another offline program that could use as much information contained in the MCS binned files as possible, in order to look as if MCS was watching the atmosphere simulated by the GCM. For a given GCM variable, we assign one of the three reference variables' binning from the MCS file. At a given MCS point (longitude, latitude, pressure level and L_S bin) we have access of the average, minimal and maximal local times as well as the number N of profiles that have been gathered in the bin. We can then reconstruct such local properties (N local times, distributed in a minimum-maximum interval that is centered on the average LT) from the GCM simulations, for each sol comprised in the MCS L_S bin, and regroup all these sols in a final GCM L_S bin, at the interpolated MCS point.

The Figure 6 shows an example of the outputs from the two different methods, the MCS observer simulator and the old LT interpolation and L_S binning sequence, applied to the same GCM simulation.

GCM diagnostic variables. In addition to creating a file from the GCM runs that is geometrically and temporally similar to the MCS files, the MCS observer simulator also aims to output quantities that are directly comparable with the quantities retrieved by MCS. For dust especially, given the variables available in the input GCM file, the simulator computes a dust opacity (in km^{-1}) at 21.6µm, that can then be put into a DSO thanks to equation (3) presented above. This

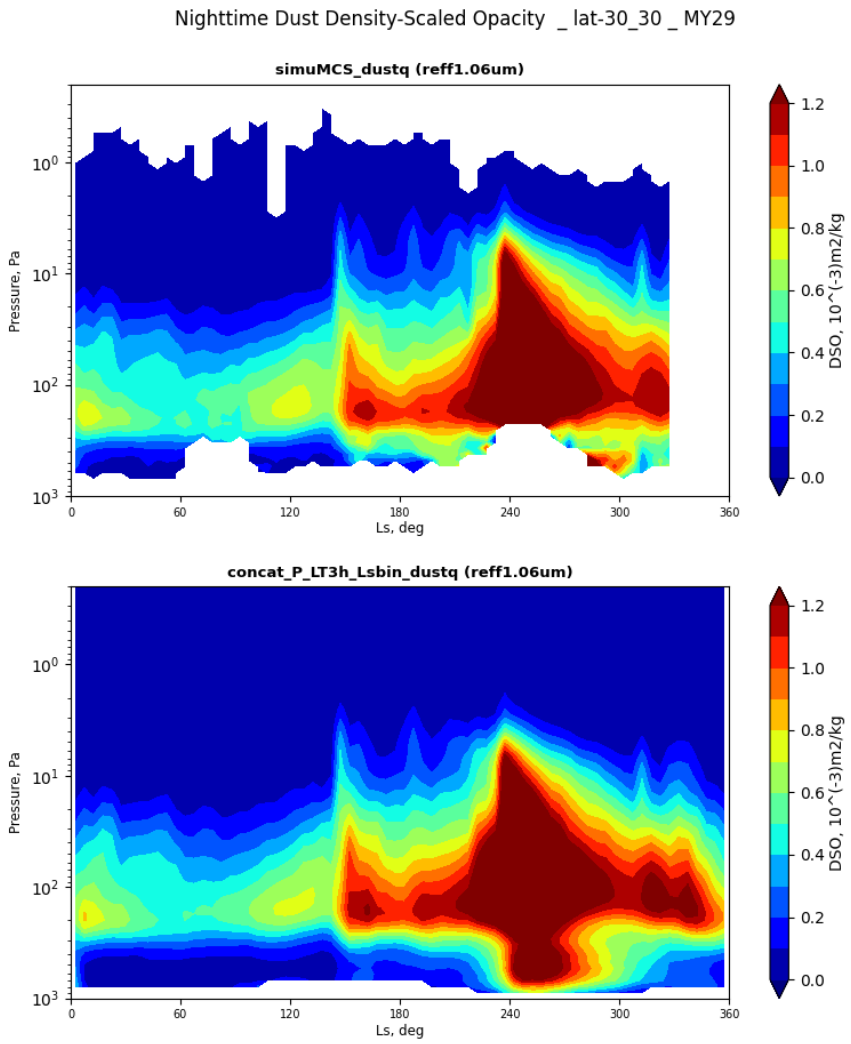

Figure 6: Outputs of the MCS simulator (Top) and the old method (Bottom) : nighttime dust Density-Scaled Opacity at 21.6µm, computed from the GCM dust mass mixing ratio via the expression from Heavens et al. [2011a] (see next paragraph) - Zonal & meridional average in latitudinal band of [-30°N;30°N] - MY29.

point requires some thinking about the diagnostic variables we should use from the GCM outputs to compare with the MCS observations.

Our first approach was to use the dust mass mixing ratio issued by the GCM, alongside the following relation taken from Heavens et al. [2011a], as it was the case in the report LMD_CNES_EXM_gcm6.0 :

$$\frac{d_z \tau}{\rho} = \frac{q}{0.012} \tag{4}$$

with the DSO in $m^2.kg^{-1}$ and q the MMR in kg_{dust}/kg_{air}. This expression, derived from a more generic equation, implies to make the same strong assumptions than those made for the retrievals of MCS soundings : an effective radius of the dust distribution r_{eff} =1.06µm, and a dust density ρ_{dust}=3000kg.m^{-3}.

These conditions, especially for the effective radius, are not representative of

the variability displayed by our model. This can particularly introduce some bias when studying a vertical distribution on which the sedimentation, for example, has a huge impact on the radius differenciation with altitude.

That's why we considered using a more precise version of the dust DSO. In the radiative transfer scheme, the GCM already computed the extinction density-scaled opacity with the actual dust r_{eff} distribution, at the IR wavelength of 9.3µm, via the generic form of the previous equation :

$$\frac{d_z \tau}{\rho} = \frac{3}{4} \frac{Q_{\text{ext}}}{\rho_D r_{\text{eff}}} q \tag{5}$$

In order to recalibrate this DSO to 21.6µm, we multiply the GCM DSO by a factor of 1.3/2.7, accordingly to Montabone et al. [2015]. The advantages of this method were limited though, because even if the r_{eff} vertical distribution was well represented within the GCM DSO, the used recalibration coefficient carried again the assumption of the effective radius of 1.06µm used by the MCS retrievals. Besides, within the physical timestep of the GCM, the radiative transfer routine is called at the beginning, before the calls of multiple other parametrizations. Hence the DSO output does not correspond to the actual dust field state at the end of the timestep. This DSO can thus be adapted to study the radiative contribution of the aerosols to the thermal tendencies, but as a proxy of the dust field itself, it would be more appropriate to use a DSO that is representative of the state at the end of the physical timestep.

Consequently, we came to create a new offline utility program, taking in input the dust MMR and effective radius from the GCM (issued at the end of the physical timestep), and computing the dust extinction opacity (km^{-1}) at the wavelength given by the user, in particular at 21.6µm. This opacity can then go through the MCS simulator like any other GCM variable, and the resulting binned opacity is eventually transformed into DSO using the MCS temperature and pressure.

Beside the discussion on the opacity's computation method, one could also consider if we should take into account in these opacities the stormdust and topdust tracers, in addition to the standard background dust (which represents the vast majority of the dust particles in the atmosphere). On the other hand, these particular dust types, whose fate is to convert into background dust at some point, could be considered computational auxiliaries only, and not used for the comparison with MCS. The subject is still an ongoing debate in the team, so we keep both possibilities in our validation studies of the GCM.

Figure 7 examplifies each method presented above, with different diagnostics of the same simulation.

NOMAD-MCS comparisons. As a complement of the MCS dust retrievals, the LMD began, in collaboration with Michael Wolff from the Space Science Institute, a work on the NOMAD observations. NOMAD is a solar occultation spectrometer suite, carried on TGO. One of its component, the spectrometer UVIS, performs measurements that enable Michael Wolff to retrieve opacity around 400-500nm, which corresponds to an extinction band of dust and water ice aerosols. He has supplied us so far with more than 4000 solar occulation profiles covering almost one Martian Year starting from L_S=180° in MY34, with quite various vertical resolutions that generally span a wide range of altitudes above areoid.

Our work then consists in finding colocalizations in longitude, latitude, L_S and local time between these NOMAD profiles and the MCS observations, with one particular aim of confirming the presence and characteristics of the *dust detached layers*. To do so, we must convert the MCS dust (21.6µm) and water ice (11.9µm) opacities into a 500nm mixed opacity. This conversion implies assuming an effective

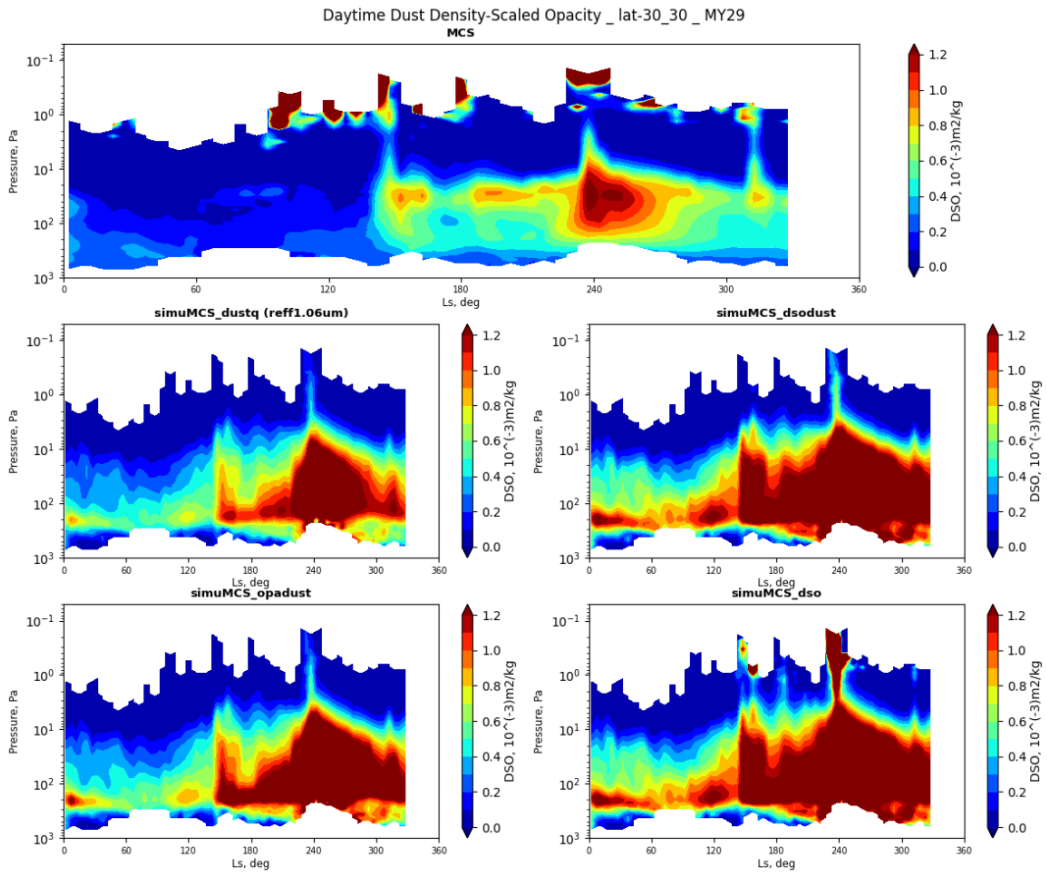

Figure 7: Daytime dust Density-Scaled Opacity at 21.6µm - Zonal & meridional average in latitudinal band of [-30°N;30°N] - MY29. **Top:** MCS data ; **Middle, left:** Opacity computed from the GCM dust mass mixing ratio via the expression from Heavens et al. [2011a] ; **Middle, right:** Opacity computed from the GCM dust DSO at 9.3µm ; **Bottom, left:** Opacity computed offline from the GCM dust mass mixing ratio and effective radius at 21.6µm ; **Bottom, right:** Opacity computed from the GCM dust+stormdust+topdust DSOs at 9.3µm

radius for each aerosol, which directly fixes the Q_{ext} ratio between the IR and visible wavelengths. This can be done either by assuming a constant r_{eff}, or by using a GCM simulation passed through the MCS simulator. The recasting of the MCS pressure grid into an altitude grid above areoid like NOMAD also requires the use of the model.

We found 150 correspondances in total, assuming a colocalization in LT for a difference of 2 hours or less. With such criteria, and given that solar occultation occurs at terminators, the matches between the two instruments can only be found at high latitudes, where MCS deviates from the 3h/15h observations (see Figure 5) and the morning and evening terminators seen by NOMAD slide away from 6h and 18h. One example is presented on Figure 8. Since this is not convenient for the study of the *dust detached layers* that are mainly tropical features on MCS observations, we also tried using MCS daytime and nighttime observations as bounds for the NOMAD profiles within the [-30°N;30°N] latitude band. This is still an ongoing work, that should bring interesting results in the near future, and should lead us to

add NOMAD observations in the validation process of the GCM too.

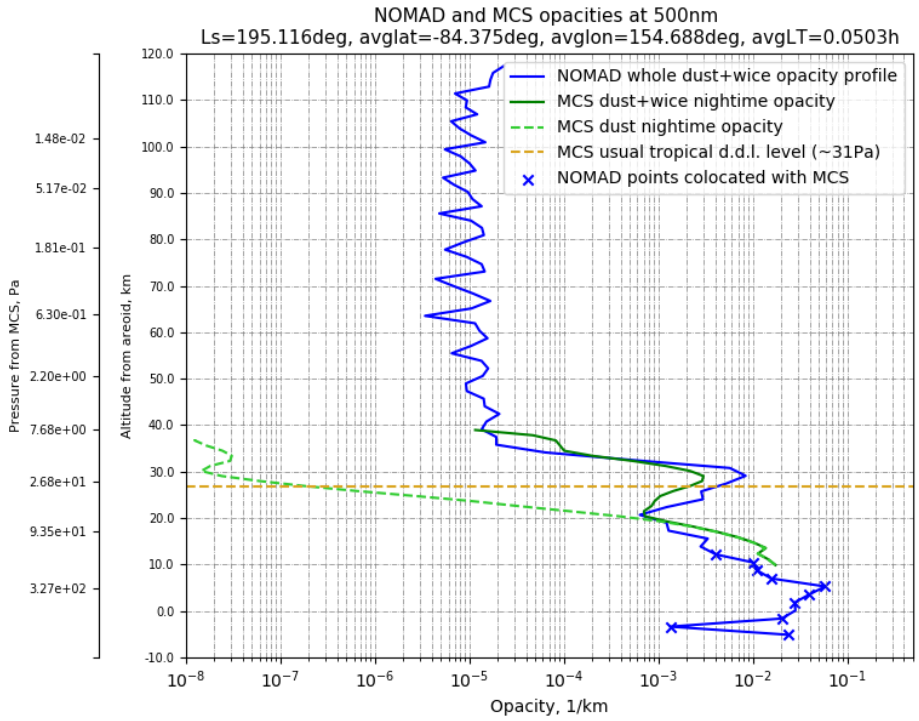

Figure 8: Example of a correspondance found between one NOMAD profile (in blue) and a nighttime MCS binned profile (in green, solid line : dust + water ice ; dashed line : dust only). The distinction done by MCS betwwen dust and water ice can be used to identify the aerosols' distribution along the NOMAD mixed opacity profile.

New injection : the CDOD as a validation tool. Finally, since the new injection scheme does not comprise anymore the normalization of the column-integrated dust optical depth to the observations, the agreement between *tau_pref_gcm* and *tau_pref_scenario* can be used as a validation tool for the tuning of the dust cycle. By quantifying the amount of dust above a given point at the surface, it can particularly serve to understand the effect of the dust vertical distribution on its horizontal transport, and identify bias linked to this new injection method.

4 Parametrizations tuning campaign

Now that we have adapted our validation methods for the GCM dust cycle, it is important to reevaluate the precedent tunings of the parametrizations. We perform comprehensive simulations, with the complete water cycle and microphysics, the scavenging by the CO_2 ice (with R=100), and we try out various combinations of some parameters of the injection, the rocket dust storm and the slope winds schemes. For consistency with previous studies (like report LMD_CNES_EXM_gcm6.0), but also because it is a quite standard year in regard to the dust events, we use dust MY29 scenario to drive our simulations.

Tuning parameters. The previous studies had already identified multiple tunable parameters that were the most relevant to impact the dust cycle.

On the dust injection scheme, a quite short timing of injection around noon seemed essential to sufficiently concentrate the stormdust to make it rise and create *dust detached layers*. However, we should also try to keep it "physical", that means coherent with the deemed context of the dust storms, which is the solar activation of the boundary layer convection that lasts a priori for a long part of the daytime. That's why we tested two injection timings : between 10h-12h and between 10h-14h.

As mentionned in Section 2, we also put a proportionnality coefficient C_{inj} before equation (1), dampening the injected dust flux. The first reason behind this coefficient is due to the method used to compute the $\Delta\tau$. Indded, when comparing the current 14h GCM CDOD with the scenario of the next day, we can not know if the difference in a given column is due to a local dust storm generating lifting, or if the dust came by the transport from adjacent columns. We put C_{inj} at 0.25 and 0.1 in the simulations.

Concerning the rocket dust storm scheme, a strong tuning factor is the detrainment coefficient C_{det}, which enables the stormdust to rise and remain concentrated for more or less time in function of its ascending speed (see Figure 2). A first sensitivity study on a wide range of C_{det}, from 0 to 1, has been performed on a simulation from L_S 120° to 180°, depicted by Figure 9, before being restrained to the two values of 0.05 and 0.02 for the whole Mars Year simulation.

As for the slope winds parametrization, simulations without the activation of this scheme have been carried out, but when it is used, one important parameter is the subgrid mesh fraction x_{mons} in which the mountain influences the aerosols' entrainment. As explained in Section 2, it depends on the height of the orography. We tried out different expressions, that are :

$$\begin{aligned}
(a) :\ x_{mons} &= 0.5\ \frac{h_{mons} - h_{min}}{h_{max} - h_{min}}\ ; \\
(b) :\ x_{mons} &= \left(\frac{h_{mons} - h_{min}}{h_{max} - h_{min}}\right)^2\ ; \\
(c) :\ x_{mons} &= \left(0.5\ \frac{h_{mons} - h_{min}}{h_{max} - h_{min}}\right)^2\ .
\end{aligned} \tag{6}$$

Expressions (b) and (c) emphasizes the influence of the high summits compared to the lower ones.

In the future, one may also look back at the detrainment coefficient of the slope winds scheme, like the rocket dust storm one. For now, the multiplicative factor before this coefficient is 1. Besides, the transport of other tracers by this process,

notably water vapor and water ice, could be a second order mitigation effect on the dust rising, via the formation of orographic clouds and the nucleation of water on the dust particles concentrated on top of the summit. This point still requires some studies to be verified though.

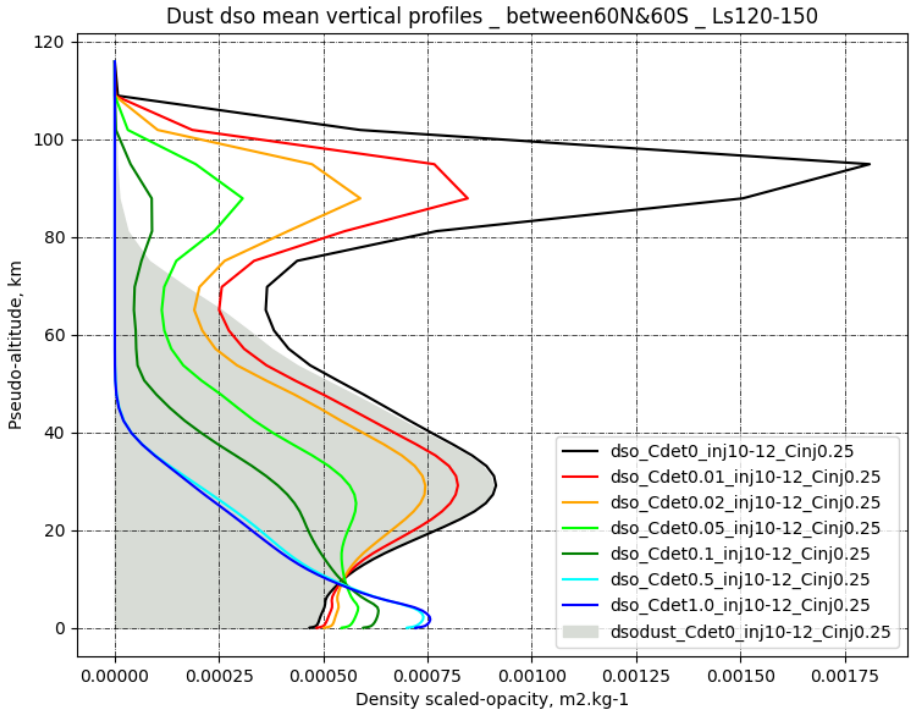

Figure 9: Dust+stormdust DSO (at 9.3µm) directly output by the GCM from the radiative transfer, for simulations with different values of C_{det} in {0., 0.01, 0.02, 0.05, 0.1, 0.5, 1.}, an injection timing between 10h-12h, with C_{inj}=0.25, and without slope winds activated. The grey area corresponds to the dust only DSO contribution for the simulation with C_{det}=0. - Zonal, meridional (in latitude band of [-60°N;60°N]) and temporal (from L_S 120° to 150°) average profiles.

Results for one MY. A first round of simulations of MY29 was performed with some of the tunings mentionned above, in order to identify the general behaviours of the new GCM dust cycle. The expression used for x_{mons} in cases where the slope winds scheme is activated, is the expression (a) from equation (6). The results are shown on Figures 10, 11, 12. The DSO plots examplified some more or less known conclusions :

- without the rocket dust storm and slope winds schemes activated, the new injection behaves quite similarly to the former GCM5.3 version (with constant injection at the surface and renormalization to the scenario) (see **"GCM5.3 nords noinj"** and **"nords inj10-12 Cinj0.25"**);
- the rocket dust storms enable the formation of elevated layers of dust during the dusty season ($L_S > 150°$), even if the "detached" characteristics is less pronounced than on MCS observations ;

- they also seem necessary to represent the occasional high-altitude peaks of dust (above 10Pa) that are observed by MCS too (with regard to simulations where they are not activated, i.e. **"GCM5.3 nords noinj"**, **"nords inj10-12 Cinj0.25"** and **"nords inj10-12 Cinj0.1 +slpwinds"**) ;

- the slope winds scheme works well at establishing a *detached dust layer* during the first half of the year, even if some simulations with strong rocket dust storms also show some potential for this (**"det0.02 inj10-14 Cinj0.25"** and **"det0.02 inj10-12 Cinj0.25"**). Yet in both cases, the dust lies a bit lower than in the MCS retrievals ;

- moreover, the slope winds accentuate the contrast between the low (P>300Pa) and mid-altitude DSO, with a clear "detached" effect on the dust, even in the stormy season when the rocket dust storms are prominent.

On the mean temperature, the use of rocket dust storms and slope winds scheme introduced a hot bias in the GCM at the mid and high altitudes where the dust is now present (see Figure 11). On the day-night thermal difference, the new dust parametrizations can influence the amplitude of the thermal tides, but have little effect of their vertical phasing, except for the simulations with the slope winds scheme activated (see Figure 12).

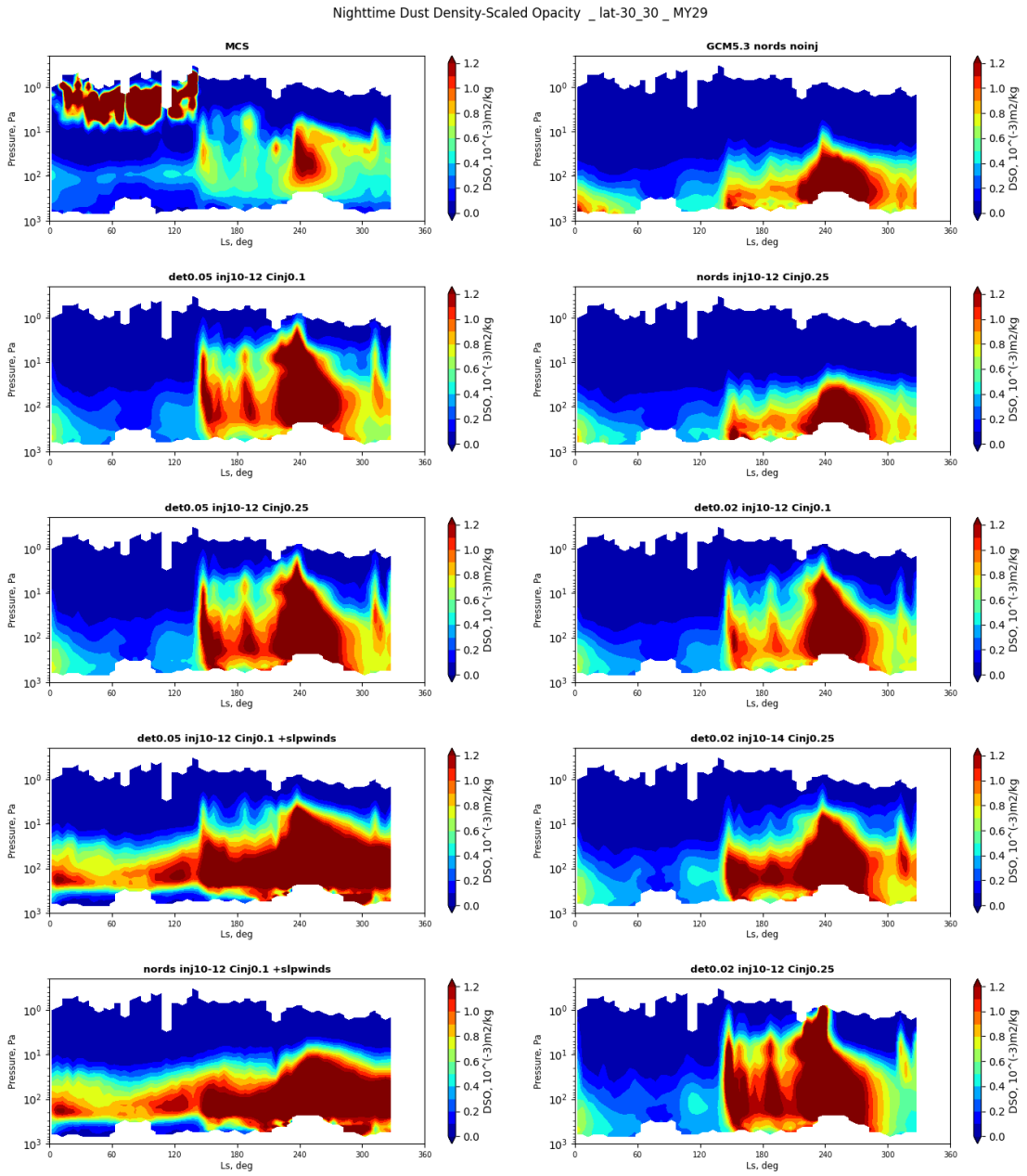

Figure 10: Nighttime dust Density-Scaled Opacity at 21.6µm (from opacity computed from the GCM dust+stormdust+topdust DSOs at 9.3µm) from MCS and several GCM simulations - Zonal & meridional average in latitudinal band of [-30°N;30°N] - MY29

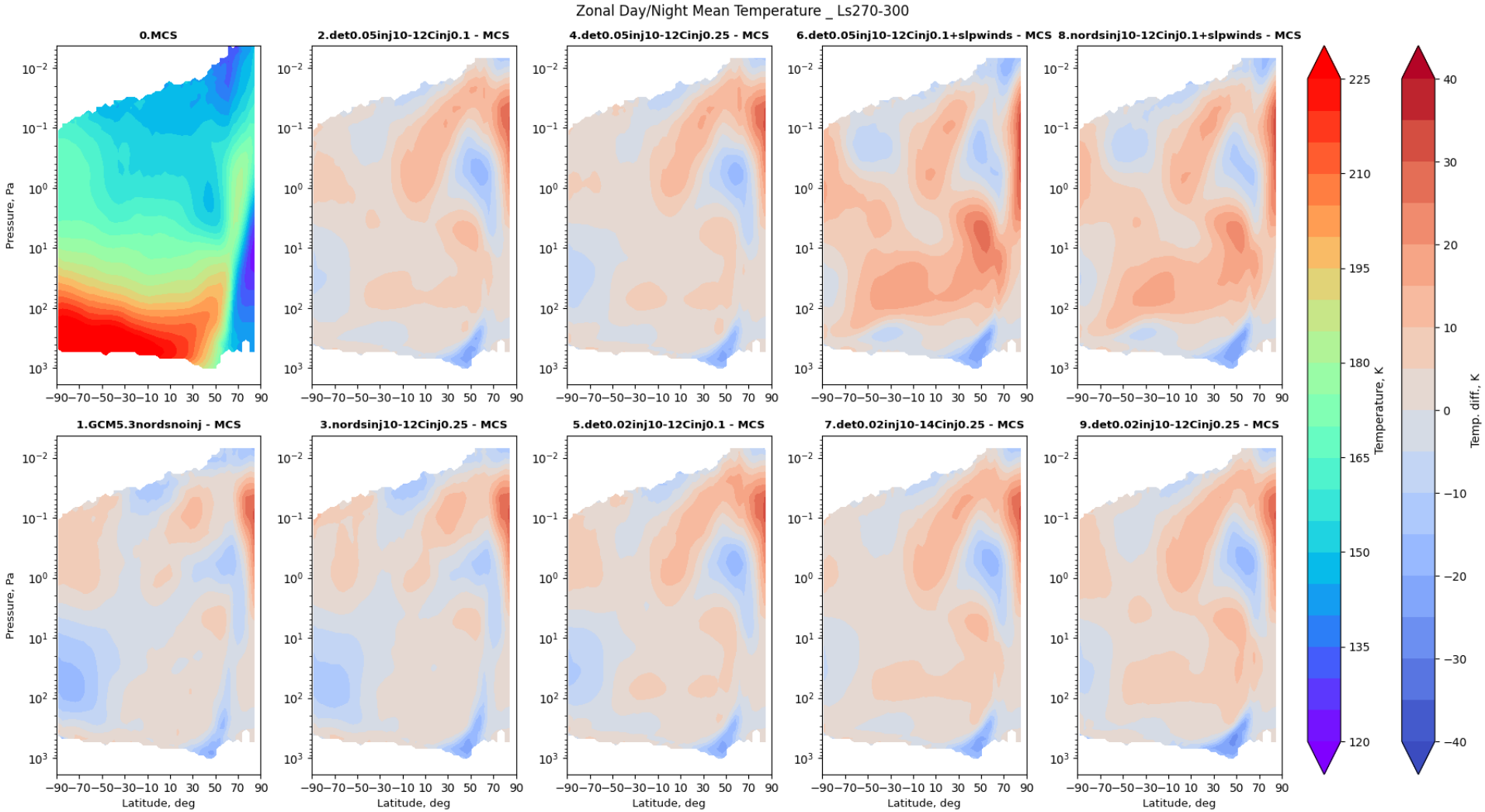

Figure 11: Mean temperature ($\frac{day+night}{2}$) from MCS (absolute value), and several GCM simulations (difference GCM-MCS) - Zonal and temporal mean from month 10 (L_S 270°-300°).

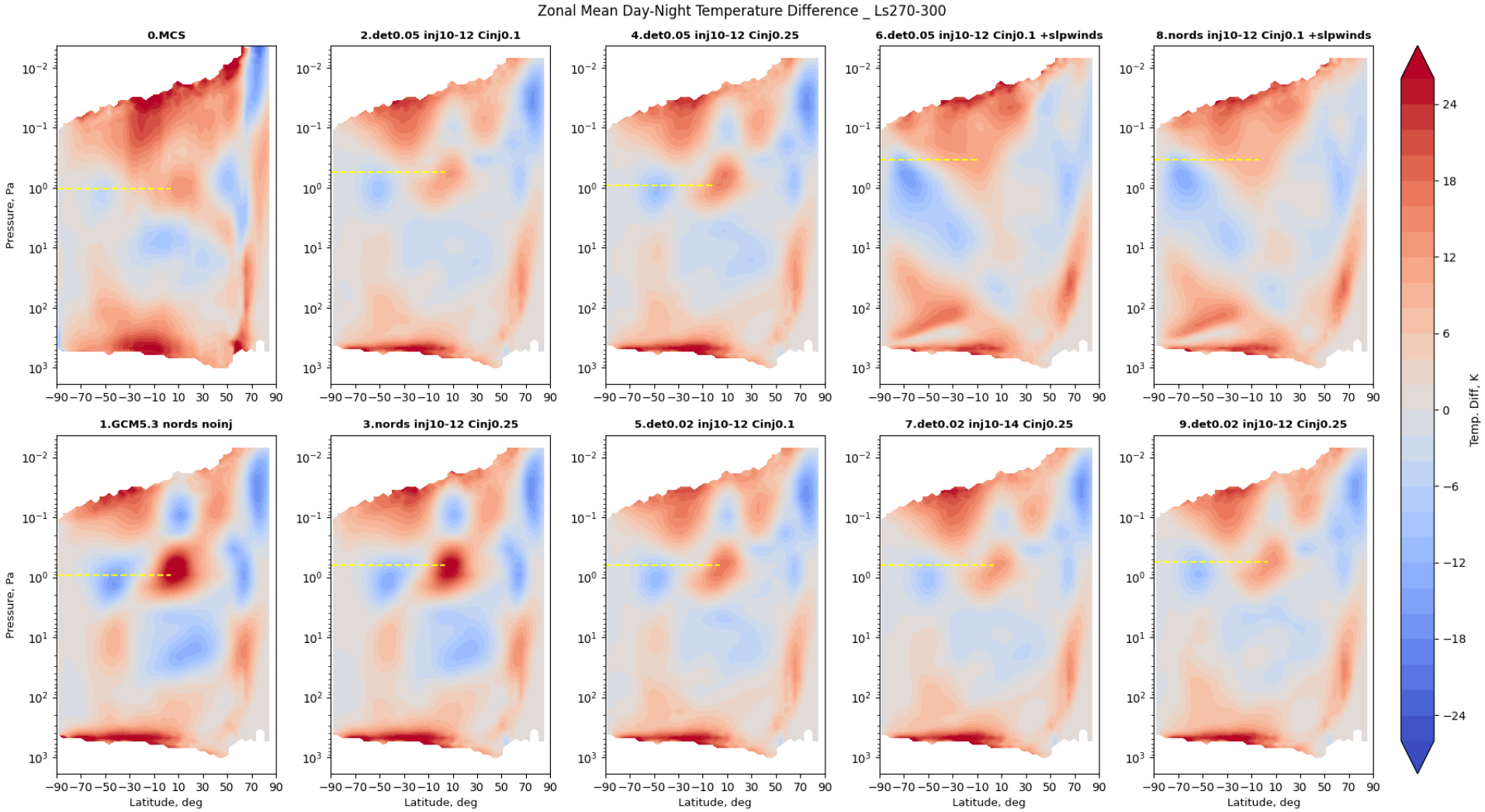

Figure 12: Temperature anomaly ($day - night$) from MCS and several GCM simulations (absolute values) - Zonal and temporal mean from month 10 (L_S 270°-300°). The yellow dashed lines mark the local maximum, underlining the vertical phasing of the thermal tides.

We then launched a second round of tuning, in order to test the different mesh fractions for the slope winds, and looked for the "best" agreement with the observations. One should notice that the DSO used in the first round for the GCM simulations was the dust+stormdust+topdust density-scaled opacity computed during the radiative transfer. It can be used to examine general behaviours, but is not really adapted for absolute comparisons with MCS, as explained in Section 3. The most adapted dust diagnostic, constructed from the dust mass mixing ratio and effective radius, is used in this second round.

The Figure 13 displays the DSO from MCS and some GCM simulations. If the change of computation for the GCM DSO has decreased a bit the final values compared to Figure 10, it appears to be still overestimated for all simulations with regard to MCS observations.

On the other hand, the comparison between the average visible column-integrated opacities from the GCM and the dust scenario seems to show a better matching, particularly for simulations **"det0.02_inj10-14_Cinj0.25"** and **"det0.05_inj10-12_Cinj0.1_slpwinds_xmons2"** (expression (b) in equation (6)), or even indicates a lack of GCM dust in some cases.

Regarding the x_{mons} tuning, the expression (c) from equation (6) seems to almost nullify the effect of slope winds when comparing simulations **"det0.05 inj10-12 Cinj0.1 + slpwinds_(0.5xmons^2)"** and **"det0.05 inj10-12 Cinj0.1"** on Figures 13 and 14. The expression (b) (simulation **"det0.05 inj10-12 Cinj0.1 + slpwinds_xmons^2"**) have a lower dampening effect, almost reaching a reasonable amplitude for this DSO diagnostic between L_S 0° and 150°. None of the mesh fraction tunings achieve to heighten the altitude of the *dust detached layers* though.

Hence, despite some promising progress made compared to the GCM version 5.3 on the dust vertical distribution, we have failed so far to find a "perfect fit" to the observations. Our studies of these new parametrizations also highlighted some systematic questionning features, like the opposition of the GCM agreements with the MCS vertical profiles and the scenario CDOD.

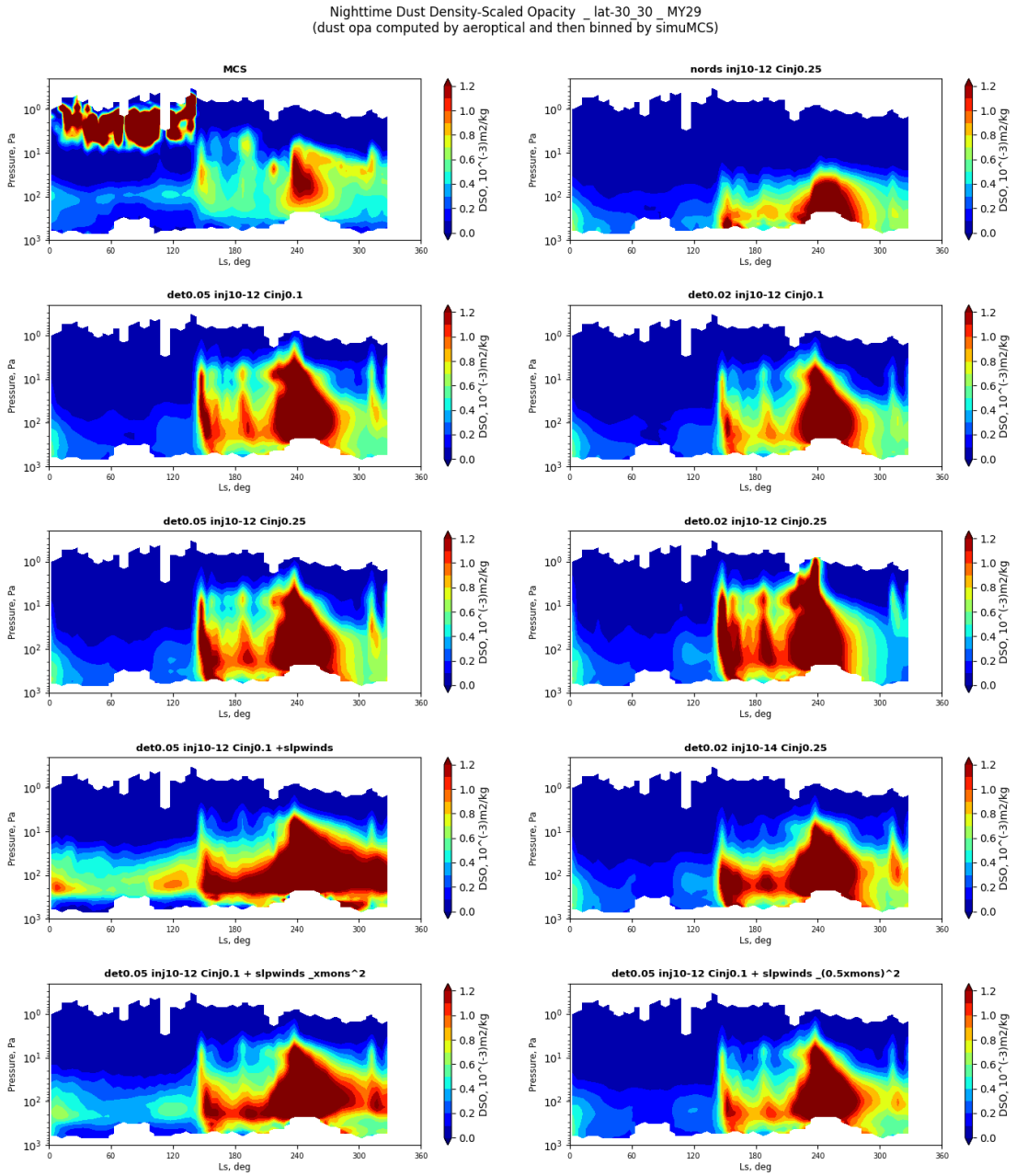

Figure 13: Nighttime dust Density-Scaled Opacity at 21.6µm (from opacity computed from the GCM dust mass mixing ratio and effecrive radius) from MCS and several GCM simulations - Zonal & meridional average in latitude band of [-30°N;30°N] - MY29

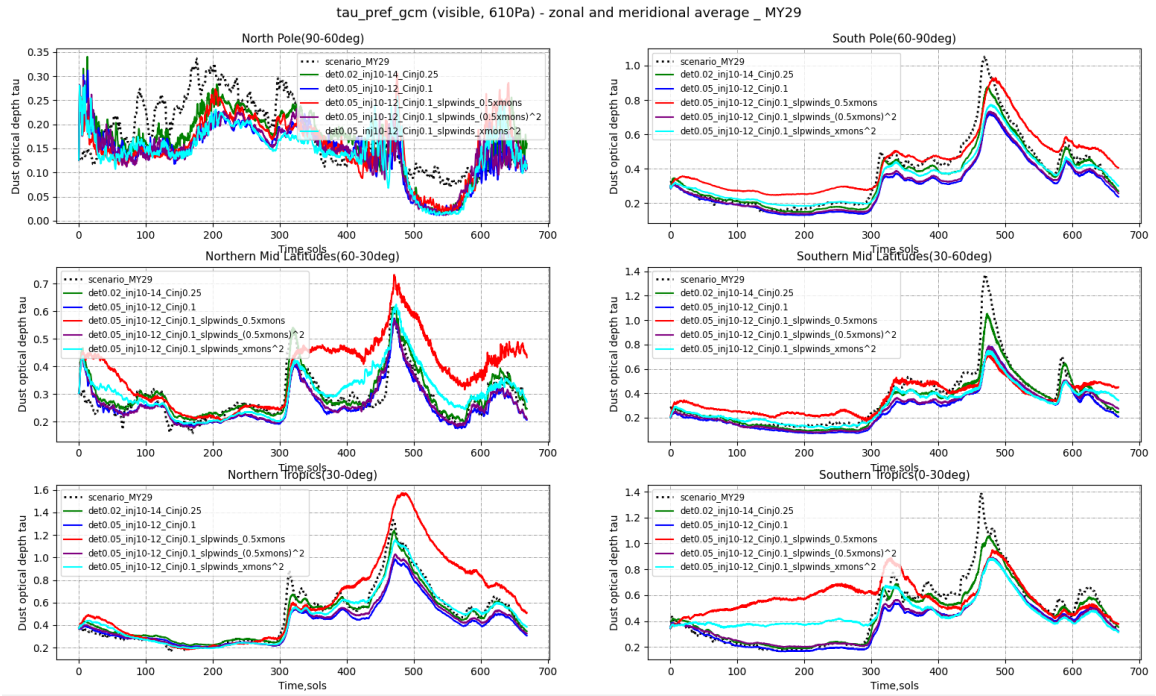

Figure 14: MY29 temporal evolution of the column-integrated dust optical depth from the observation scenario (dotted black lines) and several GCM simulations (colored solid lines) - Zonal & meridional average in latitude bands.

5 An unresolved mystery : the high-altitude storm dust

Another interrogation raised by our dust cycle studies is the systematic presence of a peak in stormdust DSO around an altitude of 80km (see Figure 9 for instance).

After investigation, no specific bug was found in the GCM code, even though some details in the sedimentation scheme may be suspicious. Actually, the presence of such a peak may be due to the very low value of the atmospheric density at such altitude, more than because of a huge quantity of stormdust. The Figure 15 examplifies this interpretation, but also reveals a surprising non-negligible density of stormdust at 60km and its associated peak of DSO.

The presence of dust at such altitudes seems quite surprising to us with regard to the common knowledge and observations of Mars atmosphere. For instance Kleinböhl et al. [2015] had ruled out this possibility in the interpretation of MCS top altitudes observations. An examination of NOMAD soundings, which cover a wider altitude range, could be used to support or infirm these observations.

This could reveal a corrupted functionning or an irrealistic representation from our rocket dust storm scheme, so we stay attentive to the question as we continue developing the model.

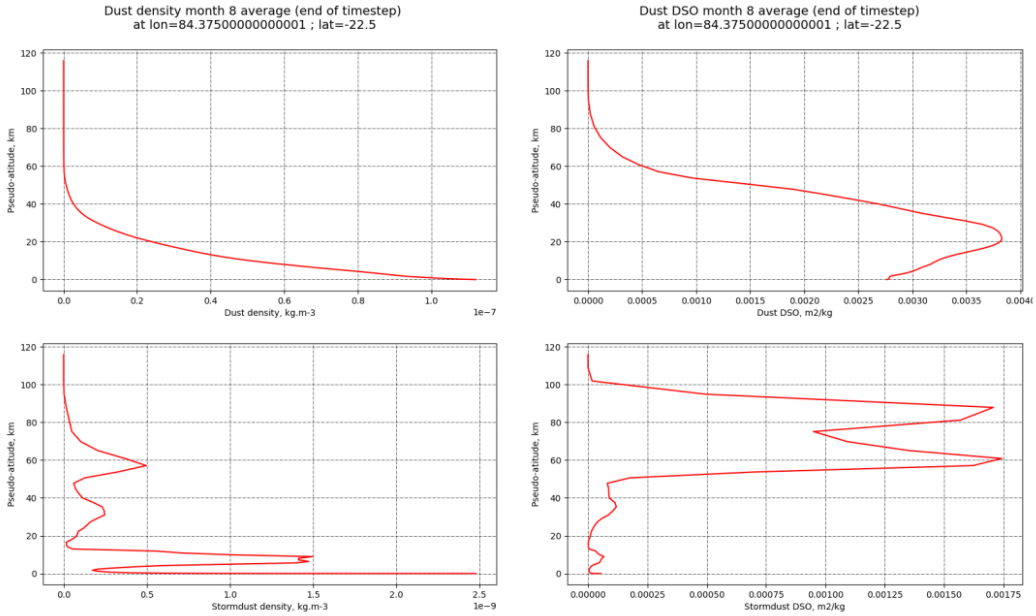

Figure 15: Study of the high-altitude stormdust on a local grid point (∼84°E,22°N) during L_S 210°-240°. **Left column:** dust volumetric mass (in kg_{dust}/m^3_{air}) ; **Right column:** density-scaled opacity computed from MMR and r_{eff} (in $m^2.kg^{-1}$) ; **Top row:** Background dust ; **Bottom row:** Storm dust

6 Dust scaling mode

Given the high DSO displayed by the GCM, we adapted our strategy and put some stronger controle from the observations back in the dust cycle. The goal here is to prevent the dust radiative impact to deregulate the atmospheric thermal structure, at least by the time we obtain a better agreement with the observed dust fields.

To do so, we implemented a new dust scaling mode that is less constraining than the GCM 5.3 full "tauscaling" but uses the same principle. At 14h locally, we evaluate the target dust scenario opacity for the next sol and compute a scaling factor :

$$dust\_rad\_adjust = \frac{\tau_{pref,scenario}(sol+1, 14h)}{\tau_{pref,gcm}(sol, 14h)} \tag{7}$$

This scaling factor is then applied to all the dust types opacities (background dust, stormdust and topdust) before computing the radiative transfer.

In order to preserve the dust daily cycle and prevent "jumps" of dust_rad_adjust at 14h, the coefficient is actually smoothed by linear interpolation, between the current sol at 14h and the next sol at 14h, when it will finally take its computed value.

Figures 16, 17 and 18 respectively show the average dust_rad_adjust, the local tau_pref_gcm evolution[10] and the mean temperature for a simulation with the new injection (timing 10h-14h, C_{inj}=0.25), the rocket dust storms (C_{det}=0.02), and with the activation of dust_rad_adjust (dustscaling_mode=2) or not (dustscaling_mode=0, like in Section 4).

[10]Note that there is no daily cycle in scenarios, since they contain only one value per sol. New versions of the scenarios, with 4 values per sol, could be produced very soon by Luca Montabone, and be used for offline validation of the GCM daily cycle. However, it is deemed inappropriate for now to use these refined scenarios as inputs for the dust injection or the dust scaling mode.

If dust_rad_adjust can locally strongly diverge from unity, especially in the polar regions where the dust opacity is very low, it remains quite close to 1. in average. This is also shown by Figures 17 and 18 where the values hardly differ from the simulation without dust_rad_adjust.

Hence it appears once more that we have a discrepancy between what the visible dust column and the vertical infrared opacity tell us. For now, two possibilities appear and we will carry on the investigations : either there is an incoherence between the scenarios (that are partly constructed from MCS data) and MCS opacity retrievals ; or maybe a bad representation of the effective radius in the model could lead us to such mismatch when comparing with both visible and infrared data.

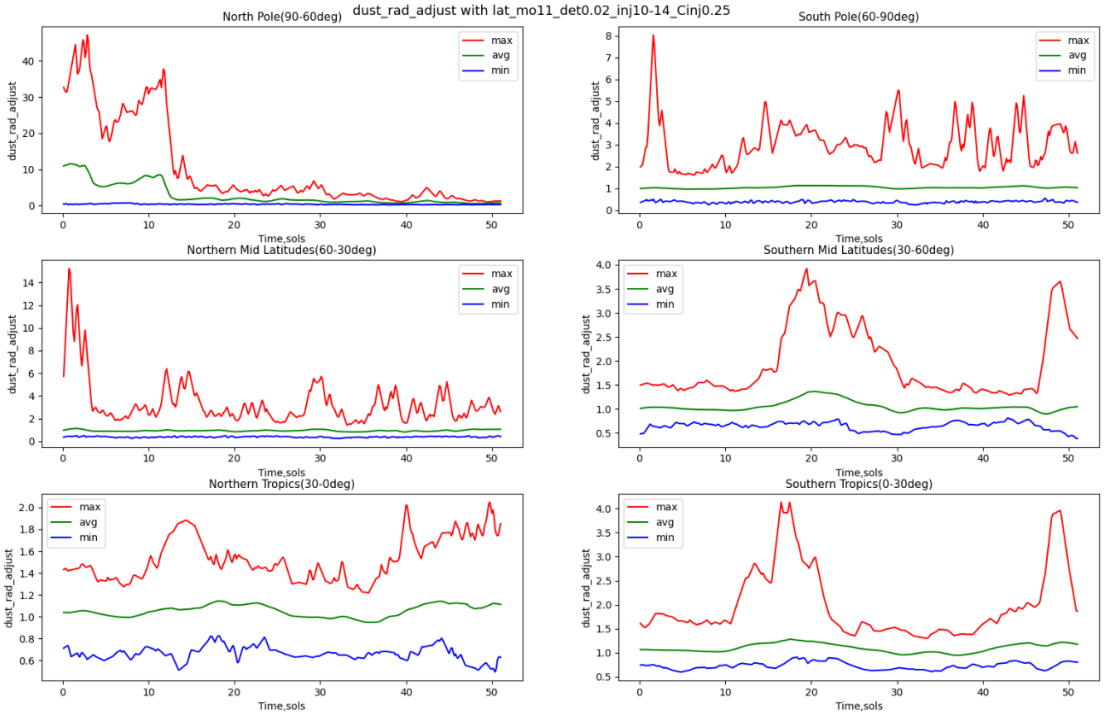

Figure 16: Zonal and meridional maximum, average and minimum values of dust_rad_adjust in bands of latitude from our simulation with dustscaling_mode=2. L_S 300°-330°

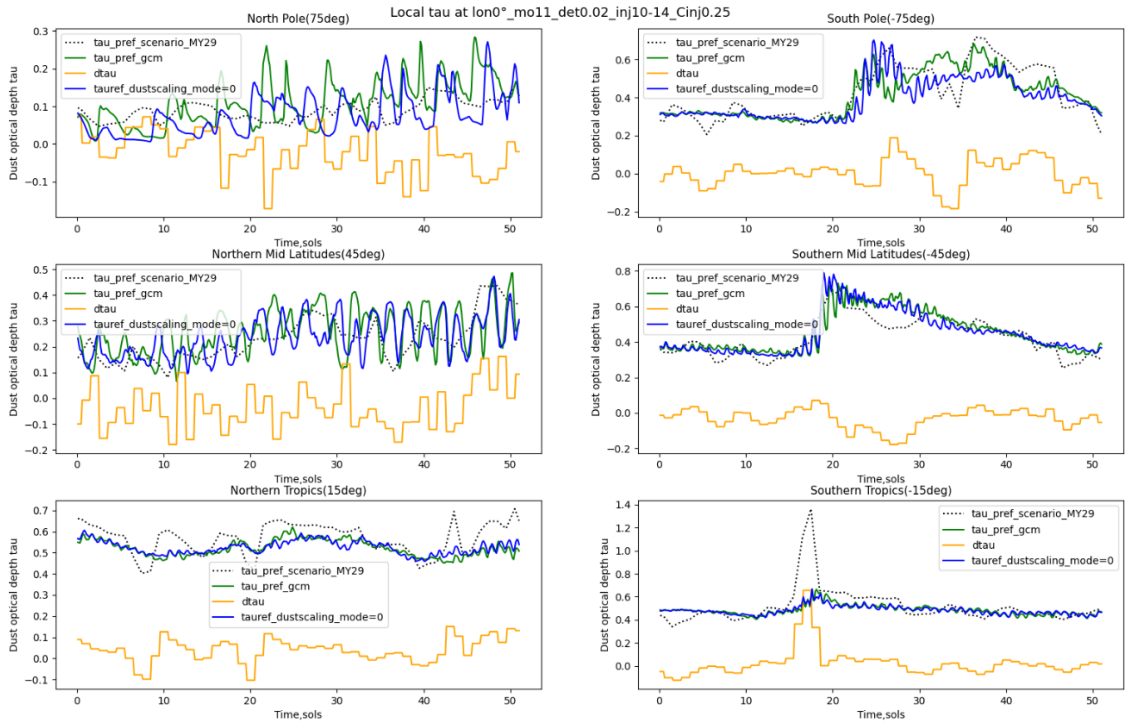

Figure 17: MY29 temporal evolution of the column-integrated dust optical depth from the observation scenario (dotted **black** lines) and GCM simulations (dustscaling_mode = **2** and **0**) at the local points of longitude 0° and latitudes ±75°, ±45° and ±15°, between L_S 300° and 330°. The yellow solid line represents the local tau difference computed each sol at 14h for the injection.

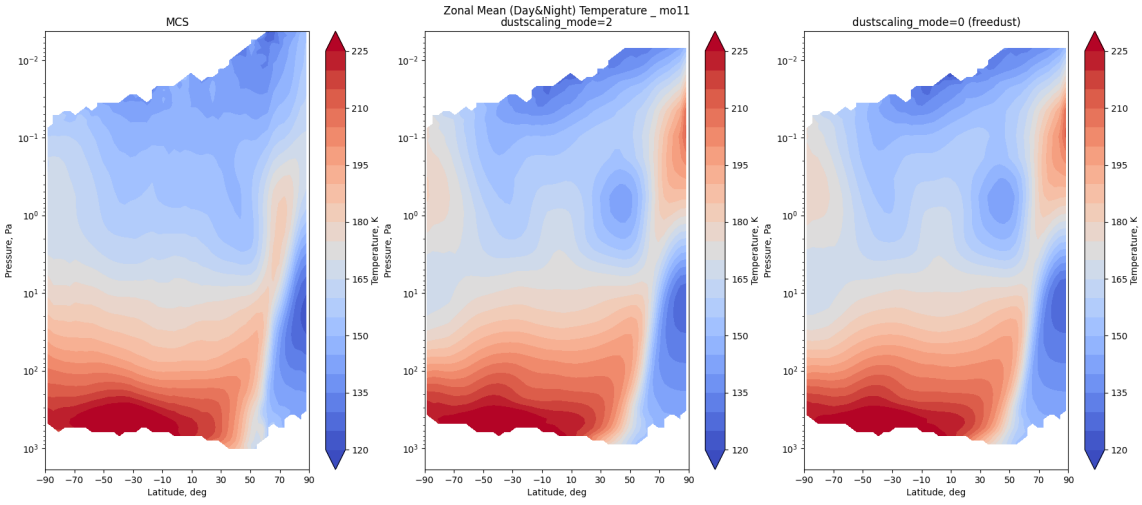

Figure 18: Mean temperature ($\frac{day+night}{2}$) from MCS and GCM simulations (dustscaling_mode = 2 and 0) - Zonal and temporal mean from month 11 (L_S 300°-330°).

7 Conclusion

Year 2020 has been the time of a profound scrutiny of the dust cycle, with the aim to have a better dust distribution for the upcoming version 6.1 of the GCM than versions 6.0 (with new parametrizations but incomplete tuning) and 5.3 (old dust cycle).

Thanks to the past developments of new parametrizations, we made a first step into a dust cycle modelization that was much more realistic, but also more open to flexible Mars conditions, with a will to let the dust freely evolve with the physics and be less constrained by the scenarios. Paradoxically, this can be achieved only by ensuring that the physical model is representative of the observed conditions, and to that matter, the model required some improvements.

A part of these improvements relies on a validation method that gets closer to the observations, by trying to reproduce the instrument and orbiter specificities as accurately as possible when comparing the GCM to the retrievals. This implied the development of two new offline utility programs, as well as a review of the GCM dust diagnostics, in order to adapt the GCM outputs into MCS-like datasets. To push further our understanding of the observations, a step out of the modelization has also been made, with the NOMAD-MCS comparison campaign, thanks to a collaboration with Michael Wolff that we will carry on.

Finally, we tried to adjust at best the coupled contributions of the injection, rocket dust storm and mountain slope winds schemes, by identifying key parameters and looking for the best fit with several observational data. Overall, we obtain with these three processes a good agreement of the dust column, with a better dust vertical profile shape that exhibits *dust detached layers*. Despite this, some discrepancies remain whatever we do. For example, we found that the new dust cycle induces a hot bias of the GCM with regard to MCS daily mean temperature. Above all, we get opposed feedbacks from our comparisons with observational data, which will now lead us to reconsider both our model and our validation method, in order to finally produce in 2021 a satisfying version 6.1 of the Mars GCM.

References

Giuranna, M., Viscardy, S., Daerden, F., Neary, L., Etiope, G., Oehler, D., Formisano, V., Aronica, A., Wolkenberg, P., Aoki, S., Cardesín-Moinelo, A., Marín-Yaseli de la Parra, J., Merritt, D., and Amoroso, M. (2019). Independent confirmation of a methane spike on Mars and a source region east of Gale Crater. *Nature Geoscience*, 12(1752-0908):326–332.

Heavens, N. G., Richardson, M. I., Kleinböhl, A., Kass, D. M., McCleese, D. J., Abdou, W., Benson, J. L., Schofield, J. T., Shirley, J. H., and Wolkenberg, P. M. (2011a). The vertical distribution of dust in the Martian atmosphere during northern spring and summer: Observations by the Mars Climate Sounder and analysis of zonal average vertical dust profiles. , 116(E15):4003.

Heavens, N. G., Richardson, M. I., Kleinböhl, A., Kass, D. M., McCleese, D. J., Abdou, W., Benson, J. L., Schofield, J. T., Shirley, J. H., and Wolkenberg, P. M. (2011b). Vertical distribution of dust in the Martian atmosphere during northern spring and summer: High-altitude tropical dust maximum at northern summer solstice. , 116(E15):E01007.

Hourdin, F. and Armengaud, A. (1999). Test of a hierarchy of finite-volume schemes for transport of trace species in an atmospheric general circulation model. *Monthly Weather Review*, 127:822–837.

Kleinböhl, A., Schofield, J. T., Kass, D. M., Abdou, W. A., Backus, C. R., Sen, B., Shirley, J. H., Lawson, W. G., Richardson, M. I., Taylor, F. W., Teanby, N. A., and McCleese, D. J. (2009). Mars Climate Sounder limb profile retrieval of atmospheric temperature, pressure, and dust and water ice opacity. *Journal of Geophysical Research (Planets)*, 114:10006.

Kleinböhl, A., Schofield, J. T., Kass, D. M., Abdou, W. A., and McCleese, D. J. (2015). No widespread dust in the middle atmosphere of Mars from Mars Climate Sounder observations. , 261:118–121.

Montabone, L., Forget, F., Millour, E., Wilson, R. J., Lewis, S. R., Cantor, B., Kass, D., Kleinböhl, A., Lemmon, M. T., Smith, M. D., and Wolff, M. J. (2015). Eight-year climatology of dust optical depth on Mars. *Icarus*, 251:65–95.

Montabone, L., S. A. K. D. M. K. A. F. F. . M. E. (2020). Martian year 34 column dust climatology from Mars Climate Sounder observations: Reconstructed maps and model simulations. . *Journal of Geophysical Research (Planets)*, 125.

Spiga, A., Faure, J., Madeleine, J.-B., Määttänen, A., and Forget, F. (2013). Rocket dust storms and detached dust layers in the Martian atmosphere. *J. Geophys. Res.*, 118:746–767.

Van Leer, B. (1977). Towards the ultimate conservative difference scheme : IV. A new approach to numerical convection. , 23:276–299.

Wang, C., Forget, F., Bertrand, T., Spiga, A., Millour, E., and Navarro, T. (2018). Parameterization of Rocket Dust Storms on Mars in the LMD Martian GCM: Modeling Details and Validation. *Journal of Geophysical Research (Planets)*, 123(4):982–1000.